Symplectically Integrating Close Encounters with the Sun

Harold F. Levison
Department of Space Studies, Southwest Research Institute, Boulder, CO 80302

and

Martin J. Duncan
Department of Physics, Queen's University, Kingston, Ontario, Canada K7L 3N6

ABSTRACT

We present a new symplectic algorithm that has the desirable property of being able to integrate close perihelion passages with the Sun. We have combined this algorithm with our fast and efficient algorithm for studying planetesimal dynamics and planet formation, known as SyMBA. The resulting code can symplectically integrate close encounters between **all** objects during a simulation, thus removing the main limitation of SyMBA (and related schemes). We believe that this algorithm will be a valuable tool for the study of the violent stages of planet formation.

Subject headings: celestial mechanics, stellar dynamics — methods: numerical — planetary systems — solar system: general

1. Introduction

The ability of the astronomical community to perform long-term integrations in planetary dynamics has blossomed over the last decade. This incredible increase is due in part to the availability of fast, low-cost computers. In addition, however, has been the development of sophisticated but highly efficient numerical algorithms known as Mixed Variable Symplectic (MVS) methods (Wisdom & Holman 1991, hereafter WH91; Saha & Tremaine 1992). These algorithms are over a factor of 10 times faster than conventional methods. Their availability has allowed us to routinely perform integrations of the outer planetary system for times greater than the age of the solar system.

Despite their power and their many contributions, the MVS algorithm has two severe limitations. First, it is not able to integrate close encounters between two objects in the simulation. Second, it is unable to follow most objects on high-eccentricity, small-perihelion distance orbits. Both these situations occur quite often in planet formation simulations (Levison et al. 1998) and other similar contexts (Rauch & Holman 1999).

In response to the first limitation, we developed a symplectic integrator that can handle close encounters between massive bodies in the solar system (Duncan et al. 1998, hereafter DLL98). This technique, known as *SyMBA*, is based on a variant of the standard MVS method, but it handles close encounters by employing a multiple timestep technique (Skeel & Biesiadecki 1994). When the bodies are well separated, the algorithm has the speed of MVS methods, and whenever two bodies suffer a mutual encounter, the timestep for the relevant bodies is recursively subdivided to whatever level is required. This algorithm is fast, efficient, and symplectic. Chambers (1999, hereafter C99) has since developed a similar integrator for handling close encounters that uses many of the concepts developed in DLL98, but applies them in novel ways. Unfortunately, neither of these techniques can handle close perihelion passages with the Sun.

There are two basic problems that cause this inability to integrate small perihelion passages. The most severe occurs because of the structure of the integrators themselves. These methods get their speed because they are derived from Hamiltonians where one term (typically the Kepler term) dominates over the others (for example, see §2). This allows for a relatively large timestep compared to more standard integrators. However, when most objects get close to the Sun, the usually small terms in the Hamiltonian can get large and the integrator fails. This problem was discussed in DLL98. Recently, Rauch & Holman (1999) discovered a more subtle problem with close perihelion passages. They showed that problems can occur if the perturbations on the Kepler orbit are not sufficiently resolved during perihelion passage.

Here we present a method for solving the problem that these integrators have with small perihelion distances. Since in §4 we show the the problem discussed by Rauch & Holman (1999) does not significantly affect our integrator with the timesteps of interest, we concentrate on redistributing the terms in the Hamiltonian so that one is always significantly larger than the rest. We accomplish this by employing some of the novel ideas developed in C99 to a different part of the Hamiltonian. In what follows, we assume a working knowledge of MVS methods in general, and SyMBA in particular. We presented a review of this topic in DLL98. The paper proceeds as follows. In §2, we briefly describe the *Democratic Heliocentric* method, which is the backbone integrator used by SyMBA. In §3 we present modifications to the Democratic Heliocentric method that will allow for small perihelion passages. Tests of this new algorithm are presented in §4. Further refinements are presented in §5. Our conclusions are presented in §6.

2. The Democratic Heliocentric Method

The Democratic Heliocentric (DH) method is a basic MVS-like algorithm that is employed by SyMBA. It has properties not contained in the original MVS that allow us to integrate close encounters (see DLL98 for a discussion). As with all of these methods, the first step in the development of the DH method is to split the Hamiltonian of the problem into two or more parts: $H = H_{\rm Kep} + H_{\rm Sun} + H_{\rm int}$, where

$$H_{\rm Kep} = \sum_{i=1}^{n} \left(\frac{|\boldsymbol{p}_i|^2}{2m_i} - \frac{Gm_i m_0}{r_i} \right), \tag{1}$$

$$H_{\rm Sun} = \frac{1}{2m_0} \left| \sum_{i=1}^{n} \boldsymbol{p}_i \right|^2, \tag{2}$$

$$H_{\rm int} = -\sum_{i=1}^{n-1} \sum_{j=i+1}^{n} \frac{Gm_i m_j}{|\boldsymbol{q}_i - \boldsymbol{q}_j|}, \tag{3}$$

where $\boldsymbol{q}_i$ and $\boldsymbol{p}_i$ are the *heliocentric* position and *barycentric* momentum [1] of body i, m_i is the mass of body i, r_i is the magnitude of $\boldsymbol{q}_i$, and m_0 is the mass of the Sun.

For the above Hamiltonian, we can construct a second-order single timestep symplectic integrator of the form

$$E_{\rm Sun}(\tau/2)\, E_{\rm int}(\tau/2)\, E_{\rm Kep}(\tau)\, E_{\rm int}(\tau/2)\, E_{\rm Sun}(\tau/2). \tag{4}$$

The algorithm is thus:

1. Each body takes a linear drift in position of the amount $\frac{\tau}{2m_0} \sum \boldsymbol{p}_i$.
2. Each body receives a kick to its momentum due to the gravitational force of the other bodies (except the Sun) in the system for $\tau/2$.
3. Each body evolves along a Kepler orbit for time τ.
4. Each body again receives a kick to its momentum for $\tau/2$.
5. Each body again takes a linear drift in position.

In general, it is possible to take large timesteps with the DH integrator because H_{Kep} is usually large compared to H_{Sun} and H_{int}. However, the integrator breaks down if one of the objects suffers a close encounter with the Sun.

---

[1] We show in DLL98 that $\boldsymbol{q}_i$ and $\boldsymbol{p}_i$ are conjugate coordinates.

An example of this behavior can be found in Figure 1 (the data for this figure is taken from DLL98). To generate this figure we integrated a system consisting of the Sun, Jupiter, and Saturn. We set Saturn's inclination (relative to Jupiter's) to 90°, and varied its eccentricity $e_{\rm Saturn}$. In order to avoid close encounters between the planets, if $e_{\rm Saturn} < 0.6$, we set the argument of the perihelion of Saturn to 90°. In this geometry, Saturn's perihelion and aphelion passages occur perpendicular to Jupiter's orbit. On the other hand, if $e_{\rm Saturn} > 0.6$, we set the argument of the perihelion of Saturn to 0°. Each integration lasted for 3000 years and had a timestep of 0.15 years. The short-dashed curve in Figure 1 shows the maximum fractional energy error in this system as a function of Saturn's perihelion distance for the system integrated with the DH method. For comparison, the dotted-dash curve shows the results for the MVS method. For both integration techniques, energy conservation degrades as Saturn's pericenter distance decreases. For perihelion distances less than $\sim$ 1AU, both integrators become unusable.

We can understand heuristically why the DH method breaks down during a close approach with the Sun by investigating the expected motion of an object involved in such an encounter. We can simplify the problem by noting that the DH fails for the Kepler problem alone (see DLL98) where $H_{\rm int} = 0$. In this case the motion of the object involved in the encounter is simply a Kepler orbit about the Sun. Recall that applying $H_{\rm Kep}$ in the DH scheme requires moving the object along a Kepler orbit. However, we are using a combination of heliocentric positions and barycentric momenta. Also, in Eq(1), we are not using the reduced mass of the system. Thus, the Kepler orbit that Eq(1) is integrating is not the same as the one the particle should take and the motion of object needs to be corrected by applying $H_{\rm Sun}$. When the perihelion distance of the object is small enough, the large timesteps that we are typically taking do not apply this correction frequently enough to resolve the perihelion passage and the integrator fails.

3. The Modified Democratic Heliocentric Method

One solution to the above problem is to modify the DH method by splitting the Hamiltonian differently. In particular, it is possible to take $H_{\rm Sun}$ and slowly and smoothly incorporate it into $H_{\rm Kep}$ during an encounter with the Sun. For example, we have developed the following splitting:

$$H'_{\rm Kep} = \sum_{i=1}^{n} \left(\frac{|\boldsymbol{p}_i|^2}{2m_i} - \frac{Gm_i m_0}{r_i} \right) + \frac{1}{2m_0} \left| \sum_{i=1}^{n} \boldsymbol{p}_i \right|^2 F(r_1, \ldots, r_n), \tag{5}$$

$$H'_{\rm Sun} = \frac{1}{2m_0} \left| \sum_{i=1}^{n} \boldsymbol{p}_i \right|^2 \left[1 - F(r_1, \ldots, r_n) \right], \tag{6}$$

$$H_{\rm int} = - \sum_{i=1}^{n-1} \sum_{j=i+1}^{n} \frac{Gm_i m_j}{|\boldsymbol{q}_i - \boldsymbol{q}_j|}. \tag{7}$$

The *global transition function*, F, is a function of the heliocentric positions of all the bodies in the system and smoothly varies from one to zero. We require F to have the following properties. First, when no object is close to the Sun, F must be zero. In this case, Eq(5) and Eq(6) are the same as Eq(1) and Eq(2), respectively, and we can just apply a normal DH step. When **any** of the objects are deep in the encounter with the Sun, we want $F = 1$. In this case, $H_{\rm Sun}$ is now totally incorporated into $H'_{\rm Kep}$, i.e. $H'_{\rm Kep} = H_{\rm Kep} + H_{\rm Sun}$ and $H'_{\rm Sun} = 0$. As an object gets close to the Sun, F must transition from zero to one. We found in DLL98 that F must be smooth in order for the integrator to be stable. As this occurs $H_{\rm Sun}$ is gradually transfered from $H'_{\rm Sun}$ to $H'_{\rm Kep}$.

We adopt the following form for F:

$$F(r_1, \ldots, r_n) = 1 - \prod_{i=1}^{n} \left[1 - f(r_i) \right], \tag{8}$$

where f is the transition polynomial developed in DLL98 but in the current application it is applied to the heliocentric distance r_i. It has the form

$$f(r_i) = \begin{cases} 1 & \text{if } r_i < R_1, \\ 10 \left(\frac{R_2 - r_i}{R_2 - R_1} \right)^6 - 15 \left(\frac{R_2 - r_i}{R_2 - R_1} \right)^8 + 6 \left(\frac{R_2 - r_i}{R_2 - R_1} \right)^{10} & \text{if } R_1 < r_i < R_2, \\ 0 & \text{if } r_i > R_2, \end{cases} \tag{9}$$

where R_1 and R_2 are constants. Figure 2 shows the behavior of f when $R_1 = 1$ and $R_2 = 2$. Note that f is everywhere smooth to its first 6 derivatives, including at R_1 and R_2.

When all objects have heliocentric distances greater than R_2, all the f's are zero, which implies that F is zero. If any one of the particles evolves to $r < R_2$ then F becomes non-zero.

If any object has $r < R_1$ then $F = 1$ and the value of F is independent of the number of objects in the *transition* region ($R_1 < r < R_2$) or *inner* region ($r < R_1$).

Note that when $F \neq 0$, $H'_{\rm Kep}$ and $H'_{\rm Sun}$ are no longer integrable. However, as C99 pointed out, it is not mathematically necessary to split the Hamiltonian into integrable parts. If one of the parts is not analytically integrable, it is possible to numerically integrate it using a standard, high accuracy integrator. For this method, we apply the Bulirsch-Stoer integrator (Press et al. 1992; although see §5) with an accuracy parameter set to 10^{-14}.

The resulting integrator has the same form as that in Eq(4). Indeed, it is the same as the DH method when $F = 0$. When an object enters the transition region, the structure of the integrator is the same as Eq(4). The only difference is that the $E_{\rm Sun'}(\tau/2)$ and $E_{\rm Kep'}(\tau)$ operations must be solved numerically.

One advantage to this solution to the problem with solar encounters is that it is trivially incorporated into SyMBA. In SyMBA, when there are no encounters between objects, it is simply the DH method. When an encounter between two objects, not including the Sun, occurs, the timestep for these two bodies is recursively subdivided to whatever level, n, is necessary to resolve the encounter. At level n, each substep involves: 1) modifying the momentum of the two objects due to their mutual gravitational attraction for a step $\tau/2n$, 2) following heliocentric Kepler orbits for these objects for time τ/n, and 3) repeating (1). Incorporating the modified DH into this scheme only requires that we replace the Kepler drift in (2) with $E_{\rm Kep'}(\tau/n)$. We must also replace all occurrences of $E_{\rm Sun}$ with $E_{\rm Sun'}$. In practice this only requires that we replace some of the subroutines.

4. Tests of Modified SyMBA

4.1. Jupiter and an eccentric planet

As described in §3, the failure of the DH method to handle close encounters with the Sun can be illustrated in a system with Jupiter and Saturn, where Saturn is placed on a very eccentric orbit. We developed this test in DLL98 in order to compare how both the DH and MVS methods fail during close perihelion passages. We have applied our new integrator to this problem, which is described in detail in §3. For this, we set $R_1 = 3AU$ and $R_2 = 4AU$ (we address how these are chosen below). The solid curve in Figure 1 shows the energy conservation for this system with the new integrator as a function of Saturn's perihelion distance. Recall that the short-dashed curve in Figure 1 shows the maximum fractional energy error in this system for the system integrated with the DH method and the dotted-dash curve shows the results for the MVS method. For this timestep, the DH and MVS integrators fail for perihelion distances less than roughly $1AU$, whereas the new algorithm can safely integrate the orbits to much smaller perihelion distances. When considering Figure 1, note that the Sun has a radius of $\sim 5 \times 10^{-3} AU$.

Chambers & Wetherill (1998) noted that during simulations of terrestrial planet formation that includes the effects of giant planets, planetary embryos can be scattered into the Sun (see also the discussion in Agnor *et al.* 1999). To test for this situation in our new algorithm, we construct a system with Jupiter on a circular orbit with a lunar-mass body on an eccentric orbit with a semi-major axis of $1AU$. We set the lunar-sized object perihelion distance equal to 0.05 AU. The integrations lasted for 10^5 years and we used a timestep of 0.015 years, which is the value used by Agnor *et al.* (1999) in their study of terrestrial planet formation.

Figure 3 shows a contour plot of the fractional change in the lunar-sized object's Tisserand parameter (which is an appropriate measure of the Jacobi constant) as a function of the locations of the transition radii, R_1 and R_2. The conservation of the Tisserand parameter is a strong function of R_2, while being a rather weak function of R_1. Given these results, one may be tempted to choose a value of R_1 close to R_2 because the algorithm is more efficient if $r < R_1$. We, however, would advice against such a course because we find that there is a long period (0.5Myr) oscillation in the Tisserand parameter with an amplitude that increases with R_1. For this problem with this timestep, we recommend using $R_1 = 0.1\,AU$ and $R_2 = 0.5\,AU$.

As we discussed in §1, Rauch & Holman (1999) discovered a problem with MVS-like integrators for small-perihelion distance orbits if the perihelion passage is not well resolved. They found that a diagnostic of this instability is that it only manifests itself if the ratio of the

orbital period of the object and the timestep of the integrator is far from a commensurability. These commensurabilities are particularly stable if the object initially was at perihelion. To test whether our integrator suffers from this problem, we repeated the above experiment keeping $R_1 = 0.1\,AU$ and $R_2 = 0.5\,AU$, but slightly changed the initial semi-major axes of the small objects so that the ratio of orbital period to dt changes.

Figure 4 shows the conservation of Tisserand parameter as a function of semi-major axis. The dotted lines show the location where the ratio of the orbital period to the timestep are integers that range from 62 for the leftmost line to 71 for the rightmost. It appears from the figure that the conservation of the Tisserand parameter is somewhat worse near the location of these resonances. A closer inspection of these data show that the peak of these errors occur just to the left of the commensurability. At the exact location of the commensurability, the Tisserand parameter is much smaller. Perhaps the location of the large errors is associated with the regions near 1:n commensurabilities where the density of commensurabilities is low. In any case, although these are regions where the accuracy of the integrator is somewhat degraded, these regions are small and the degradations are not of practical importance.

4.2. Binary Planet

As a very stringent test of the ability of the code to simultaneously handle a close encounter between objects **and** close perihelion passages, we integrated a pair of planets in a bound binary with their center of mass revolving about a star. The center of mass of the binary was placed in an orbit with a semi-major axis of 1 AU and a pericenter distance of 0.05 AU about a solar-mass star. The initial semi-major axis of the relative orbit of the binary was 0.0125 AU and the initial eccentricity was 0.6. Each planet had a mass equal to that of Jupiter. We again took a timestep of 0.015 years. We set $R_1 = 0.1\,AU$ and $R_2 = 0.5\,AU$.

Figure 5 shows the behavior of the system through its first perihelion passage. The green curve shows the distance between the two planets while the red and blue curve show their heliocentric distances. Note that the raggedness of the curves is due to poor temporal resolution which, in turn, is set by the timestep of the integration. The two planets are bound to one another until they get close enough to the Sun for the tidal stresses to rip the binary apart. Figure 6 shows the fractional change in energy during this passage. The energy conservation is quite good considering the difficulty of this integration.

4.3. The Circular Restricted 3-Body Problem

As we described above, the original version of SyMBA had difficulties if, during an integration, a small object is scattered to a small perihelion distance by a larger one. Perhaps the test that is the best analog of this situation is one where a planet on a circular orbit scatters much smaller objects. Thus, we integrated the orbits of 900 massless test particles under the gravitational effects of Jupiter and the Sun, where Jupiter was on a circular orbit at 5.2 AU. The particles were initially uniformly distributed in semi-major axes between 3 and 20 AU. If a particle had a semi-major axis less than Jupiter's then its aphelion distance was set to 5.4 AU. If, on the other hand, its semi-major axis was greater than that of Jupiter's, its perihelion distance was set to 5.0 AU. The inclinations of the particles were chosen so that their initial Tisserand parameter was 1.5. The longitudes of the ascending nodes, arguments of perihelion and mean anomalies of the particles were all set to zero. The system was integrated for 10^4 years with a timestep of 0.05 years. We set $R_1 = 0.1$ AU and $R_2 = 2.0$ AU.

Figure 7 shows the maximum fractional deviation of the Jacobi constant of a particle as a function of the smallest perihelion distance it obtained during the integration. The blue points show this result when the integration was performed with the old version of SyMBA. Note the large systematic decrease in performance for smaller perihelion distances. Indeed, in many cases with minimum perihelion distances less than ~ 0.1 AU the integrator fails (as indicated by fractional changes in the Tisserand parameter of $\gtrsim 50\%$). The red points show the results for the new algorithm, which does not show a degradation in performance for small perihelion distances.

5. Extensions to the Bulirsch-Stoer integrator

As described above, we employ the Bulirsch-Stoer method (Press et al. 1992, hereafter PFTV92) to integrate the equations of motion for Hamiltonians which are not integrable. Unfortunately, the Bulirsch-Stoer method is computationally expensive; typically being ~ 20 times slower than the normal DH method. Here we describe an attempt to increase the efficiency of the Bulirsch-Stoer method by building in knowledge of the system that we are integrating. Unfortunately, although the technique presented here works, it is usually less efficient than the standard Bulirsch-Stoer. However, refinements of these techniques may lead to more efficient implementations. Thus, we present these ideas in the hope that they may be useful in the future.

We base our discussion on the Bulirsch-Stoer method presented in PFTV92. Contrary to popular belief, the Bulirsch-Stoer method is not an integration technique, but is a method for obtaining a high accuracy result from an independent integrator. It achieves high accuracy by first taking a timestep, $\tau = \Delta t$, using this integrator. Then, using the same initial conditions as before, it makes two successive substeps with $\tau = \Delta t/2$. It continues this procedure of subdividing the step until it can safely extrapolate to an infinite number of iterations with $\tau = 0$. If the extrapolation fails, the Bulirsch-Stoer method decreases Δt and tries again. In this way, it determines its own timestep.

Thus, the Bulirsch-Stoer method must make use of another integrator. The Bulirsch-Stoer method presented in PFTV92 uses the *Modified Midpoint Method*, which is a second order integrator. However, there is no particular reason to use this integrator over other second order (or higher) integrators. Indeed, there are second order integrators, like the MVS method, that have built into them some knowledge of the system that we are integrating and may allow the Bulirsch-Stoer method to use a larger timestep.

We have found that the most CPU consuming part of the modified DH method involves applying the operator of $H'_{\rm Kep}$, see Eq(5). During a close perihelion passage, an object's orbit is best approximated by a Kepler orbit about the Sun. With this in mind, we find that we can rewrite Eq(5) as

$$H'_{\rm Kep} = \sum_{i=1}^{n} \left(\frac{|\boldsymbol{P}_i|^2}{2m_i} - \frac{G m_i m_0}{|Q_i|} \right) + \sum_{i=1}^{n} G m_i m_0 \left[\frac{1}{|Q_i|} - \frac{1}{|q_i|} \right] - \frac{1}{2m_0} \left| \sum_{i=1}^{n} \boldsymbol{p}_i \right|^2 \left[1 - F(r_1, \ldots, r_n) \right], \tag{10}$$

where $\boldsymbol{Q}_i$ and $\boldsymbol{P}_i$ are the Jacobi coordinates for particle i (see WH91). The first two terms of Eq(10) are the same as the first two terms in Wisdom & Holman's MVS method. For the first particle in the Jacobi list, the middle term is zero. Also if the innermost particle has $r < R_1$ then the last term is also zero. So during a close encounter, we are left with a Kepler

orbit about the Sun. It therefore seems natural to replace the Modified Midpoint Method in the Bulirsch-Stoer with a second order MVS-like integrator based on the three terms in Eq(10) when trying to solve $H'_{\rm Kep}$.

This method does work and is as accurate as the original. It also accomplished our goal in that it allows the Bulirsch-Stoer integrator to take larger timesteps, particularly near perihelion. Unfortunately, the MVS-like step described above takes much more CPU time then a simple Modified Midpoint Method step. The extra cost of performing the MVS-like step outweighs the advantages of the larger timestep and this new method is, in general, less efficient than the normal modified DH method in our first attempt at implementation.

6. Concluding Remarks

In DLL98 we developed a powerful new integration technique, known as SyMBA, that is fast and efficient and will symplectically integrate close encounters between massive bodies in the solar system. Such an integrator is required to perform accurate integrations of the late stages of planet formation. Unfortunately, this integrator suffers from a significant limitation: it cannot handle close perihelion passages.

Here we develop a modification to SyMBA that will allow close encounters with the Sun. We employ ideas developed in C99 which can symplectically redistribute parts of the Hamiltonian and apply them as an object approaches the Sun. As a result, close solar encounters can be integrated using the relatively large timesteps usually employed in these integrations.

During such an encounter, this new algorithm is computationally expensive since it makes use of a Bulirsch-Stoer method to solve the non-integrable parts of the Hamiltonian. For example, in a solar system containing only Jupiter and Saturn, the new algorithm required a factor of 8 times more CPU time than MVS when R_1 was beyond the orbit of the planets. However, when not integrating through a small perihelion passage, it has the speed and accuracy SyMBA. Thus, we recommend that the timestep of the integrator be chosen so that R_2 can be small enough that particles rarely enter the transition zone. In this way, during the vast majority of time, the technique has the speed of the SyMBA. However, if an object were to get scattered onto an orbit with a small perihelion distance, the integrator would not suffer a catastrophic failure and in general would retain its high accuracy.

We would like to thank L. Dones and C. Agnor for useful discussions. SyMBA was developed, in part, under a SwRI internal research grant. HFL is grateful to NASA's Exobiology and Origins of Solar Systems programs for funding. MJD is grateful for the continuing financial support of the Natural Science and Engineering Research Council of Canada.

REFERENCES

Agnor, C.B., Canup, R.M., & H. F. Levison 1999, Icarus, 142, 219

Chambers, J.E. 1999, MNRAS, 304, 793

Duncan, M.J., Levison, H.F., & Lee M.H. 1998, AJ, 116, 2067

Levison, H.F., Lissauer, J.J., & Duncan, M.J. 1998, AJ, 116, 1998

Press, W.H., Flannery, B.P., Teukolsky, S.A., & Vetterling, W.T. 1986. Numerical Recipes in Fortran: The Art of Scientific Computing: Second Edition. Cambridge University Press, Cambridge.

Rauch, K.P., & Holman, M. 1999, AJ, 117, 1087.

Saha, P., & Tremaine, S. 1992, AJ, 104, 1633

Skeel, R.D., & Biesiadecki, J.J. 1994, Ann. Numer. Math., 1, 191

Wisdom, J., & Holman, M. 1991, AJ, 102, 1528

This preprint was prepared with the AAS LaTeX macros v4.0.

Fig. 1.— The maximum fractional change in energy for an integration of a system containing only the Sun, Jupiter, and Saturn as a function of Saturn's perihelion distance. Jupiter's initial eccentricity was 0.05 for all the runs. The dashed and dot-dashed curves refer to results obtained by the DH and the MVS scheme, respectively. The solid curve refers to the modified DH method.

Fig. 2.— The transition function, f, when $R_1 = 1$ and $R_2 = 2$.

Fig. 3.— Contours of the fractional change in a lunar-sized object's Tisserand parameter in a system that also contains Jupiter on a circular orbit, as a function of the locations of the transition radii, R_1 and R_2. The lunar-sized object had an initial semi-major axes of 1 AU. The integrations lasted for 10^5 years and we used a timestep of 0.015 years.

Fig. 4.— The fractional change in a lunar-sized object's Tisserand parameter in a system that also contains Jupiter on a circular orbit, as a function of the small object's semi-major axis. The dotted lines show the locations of the 1:n commensurabilities between the small object's orbital period and the timestep of the integrator. The leftmost dotted line shows the location of the 1:62 commensurability while the rightmost is the 1:71.

Fig. 5.— The temporal evolution of a system that contained two planets in a bound binary in orbit about the Sun. The binary had an initial semi-major axis of 0.0125 AU and an initial eccentricity of 0.6. The center of mass of the binary was on a sun-grazing orbit with an initial semi-major axes of 1 AU. The green curve shows the relative distance between the two planets as a function of time. The blue and red curves show the heliocentric distances as a function of time.

Fig. 6.— The variation of the energy of the system shown in Figure 5.

Fig. 7.— The maximum fractional deviation in the Jacobi constant of a massless test particle under the influence of Jupiter on a circular orbit, as a function of the smallest perihelion distance the object obtained during a 10^4 year integration. The blue and red points show this result when the integration was performed with the old and new versions of SyMBA, respectively.

Figure1 —

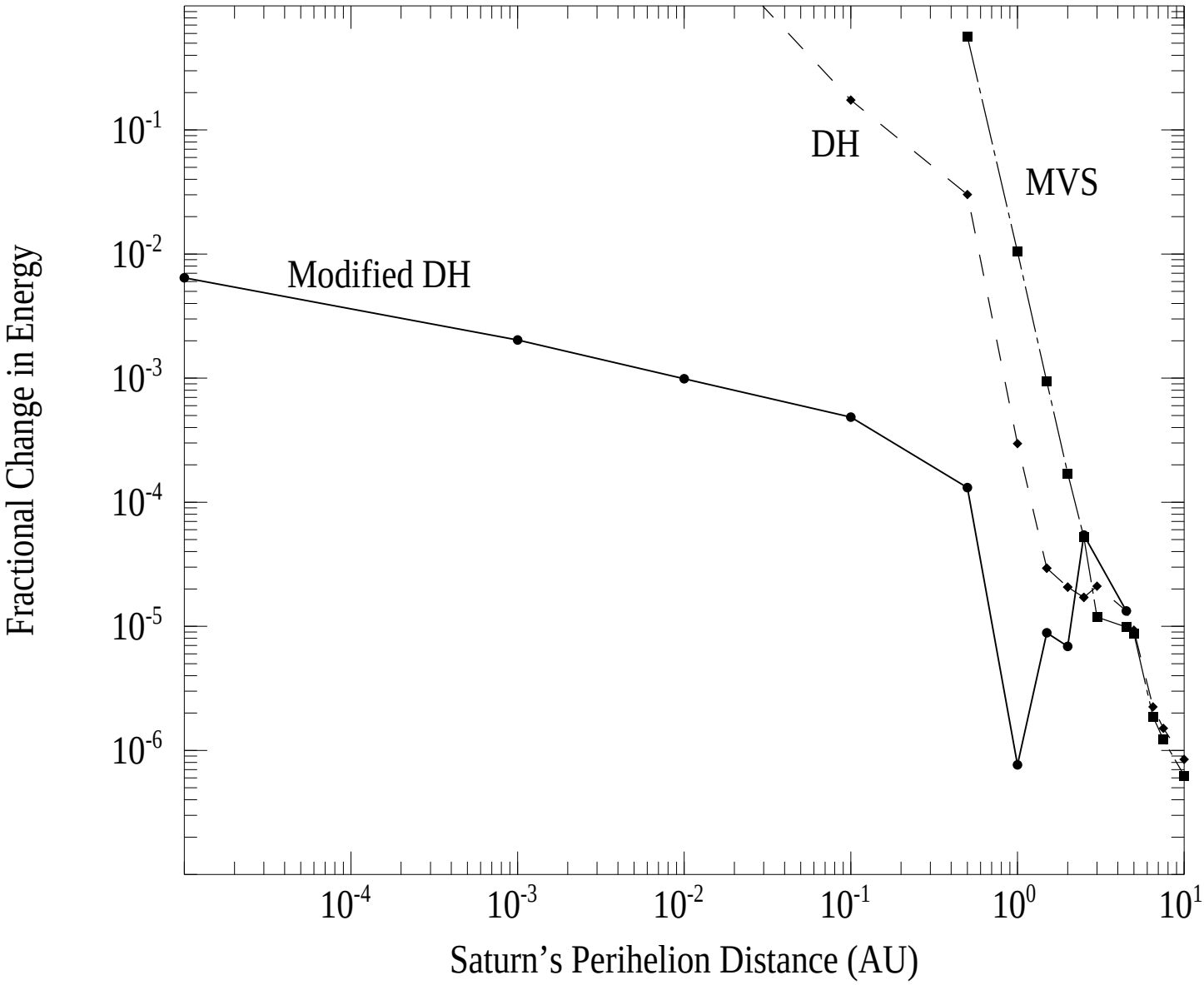
Fractional Change in Energy
10^{-1}
10^{-2}
10^{-3}
10^{-4}
10^{-5}
10^{-6}
DH
MVS
Modified DH
10^{-4}
10^{-3}
10^{-2}
10^{-1}
10^{0}
10^{1}
Saturn's Perihelion Distance (AU)

Figure2 —

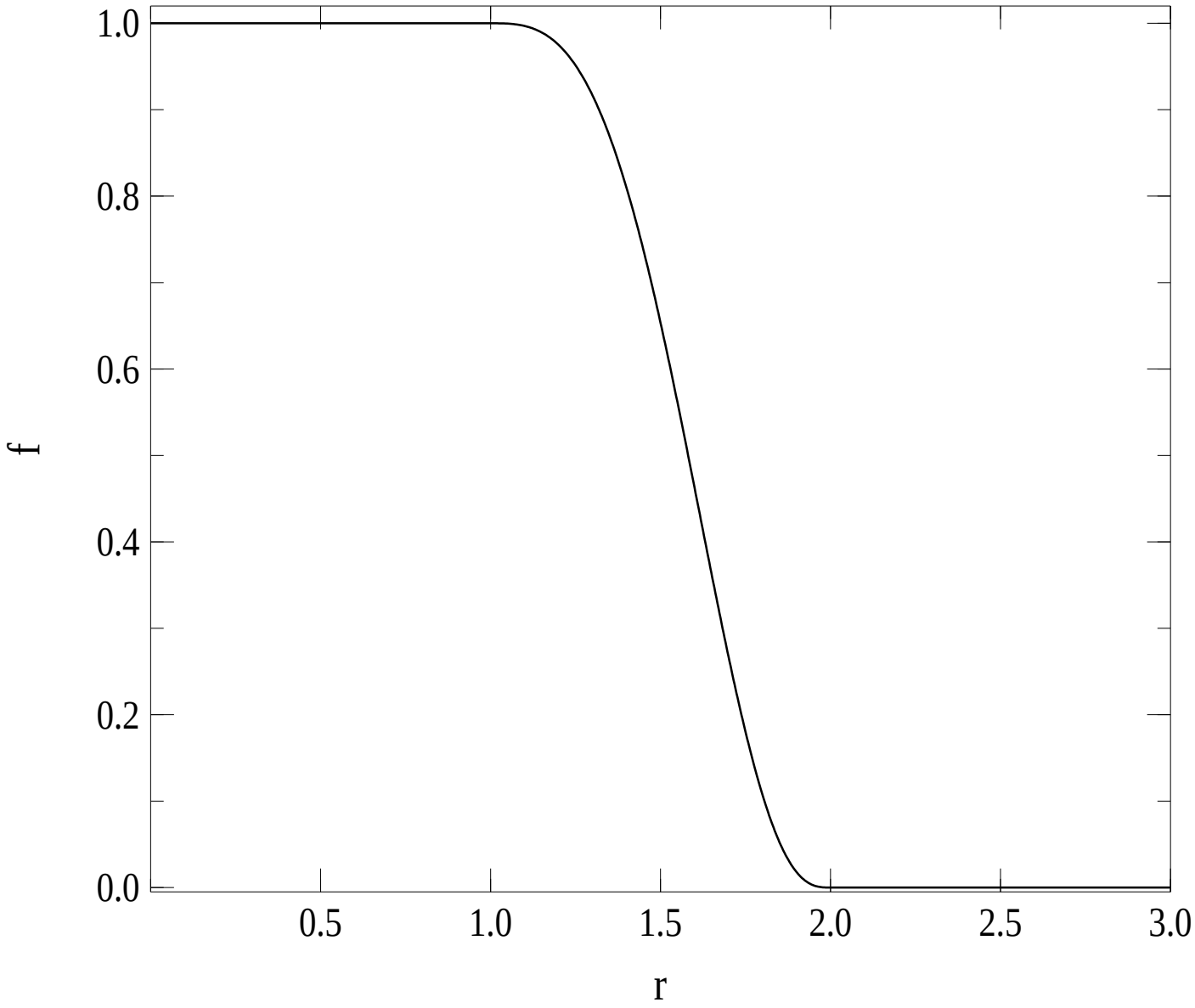

Wed Feb 23 11:03:01 2000 L.O.A. Computer Team

Figure3 —

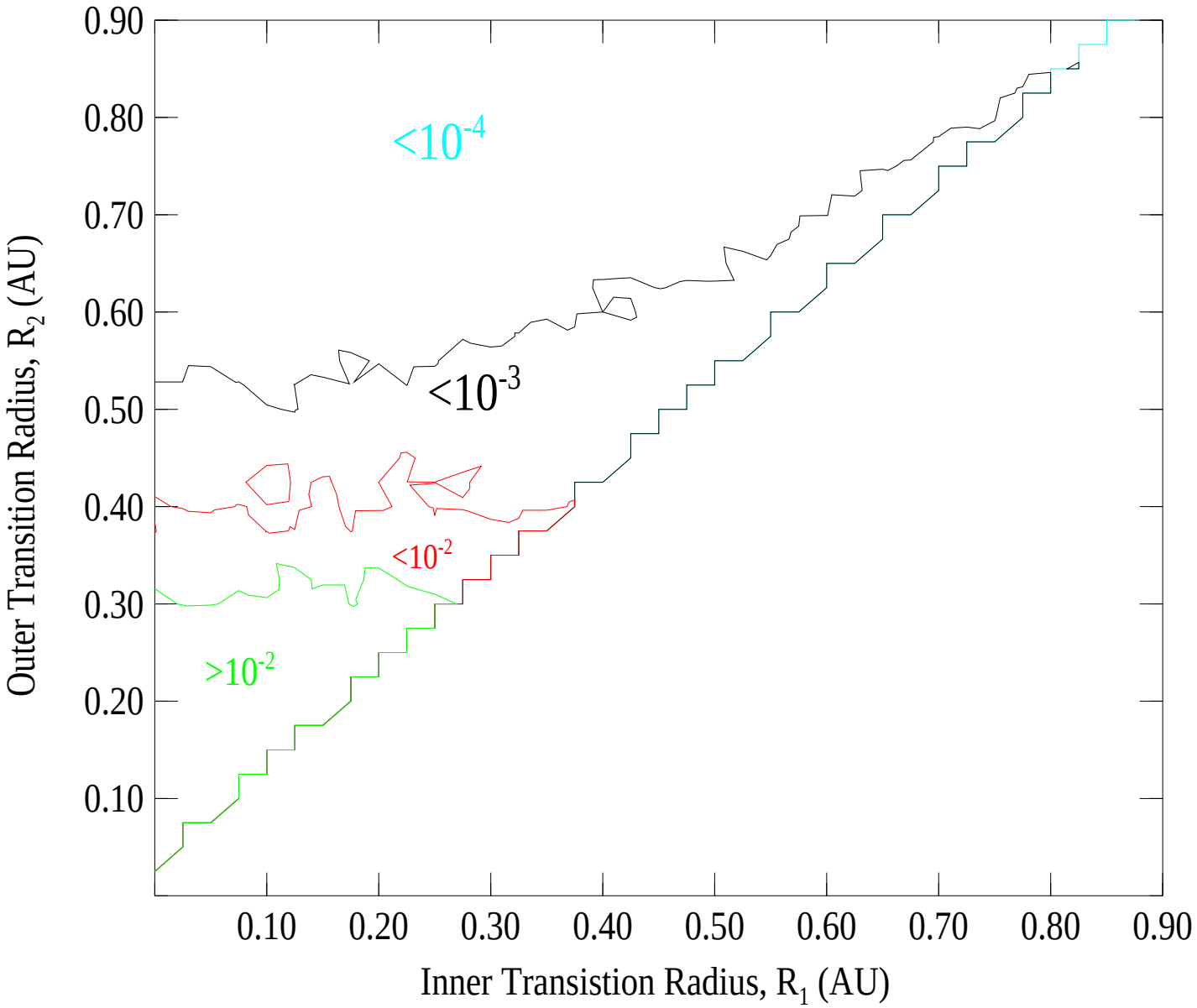
0.90
0.80
0.70
0.60
0.50
0.40
0.30
0.20
0.10
Outer Transition Radius, R_2 (AU)
$<10^{-4}$
$<10^{-3}$
$<10^{-2}$
$>10^{-2}$
0.10
0.20
0.30
0.40
0.50
0.60
0.70
0.80
0.90
Inner Transistion Radius, R_1 (AU)

Figure4 —

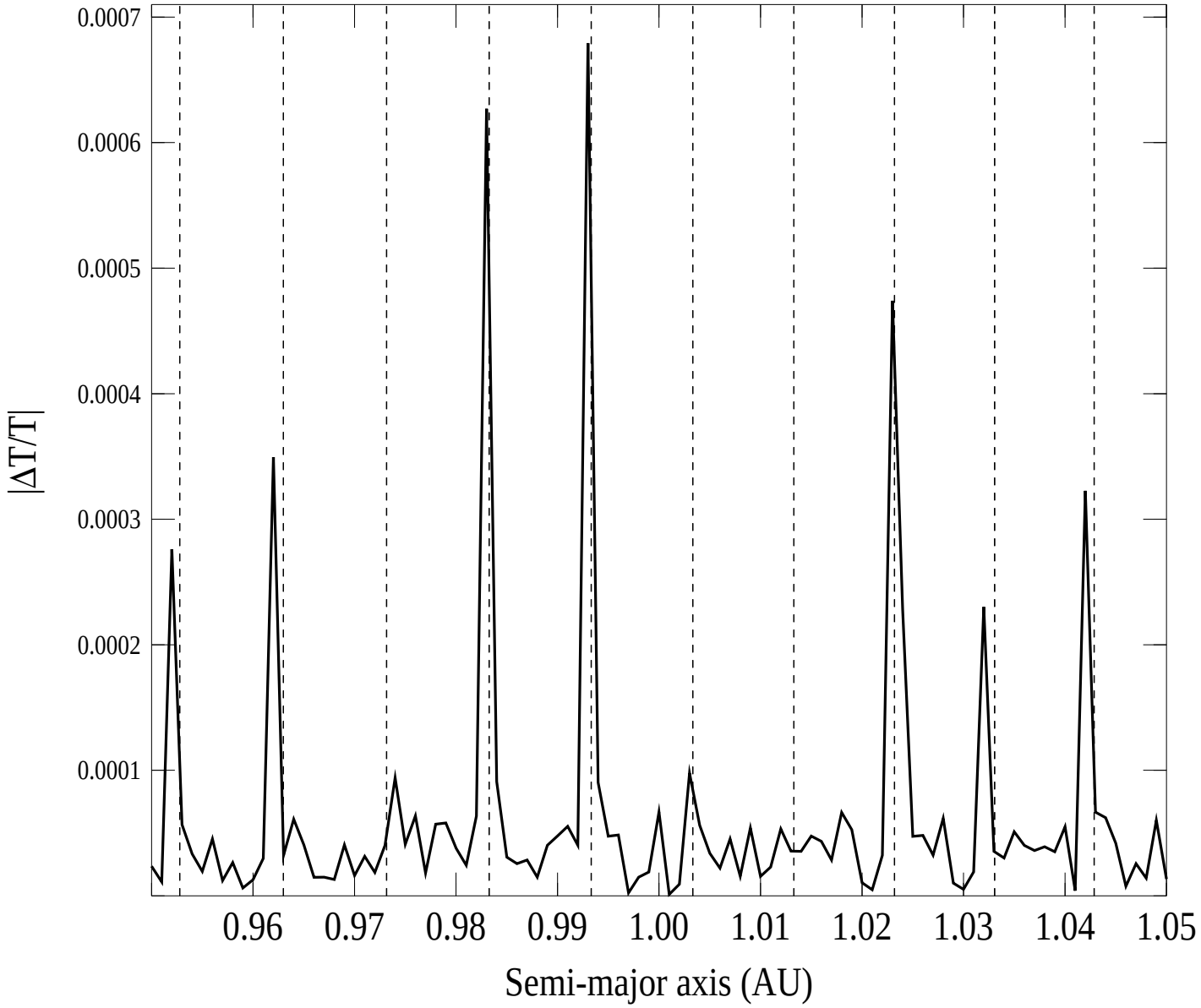
0.0007
0.0006
0.0005
0.0004
0.0003
0.0002
0.0001
|ΔT/T|
0.96
0.97
0.98
0.99
1.00
1.01
1.02
1.03
1.04
1.05
Semi-major axis (AU)

Figure5 —

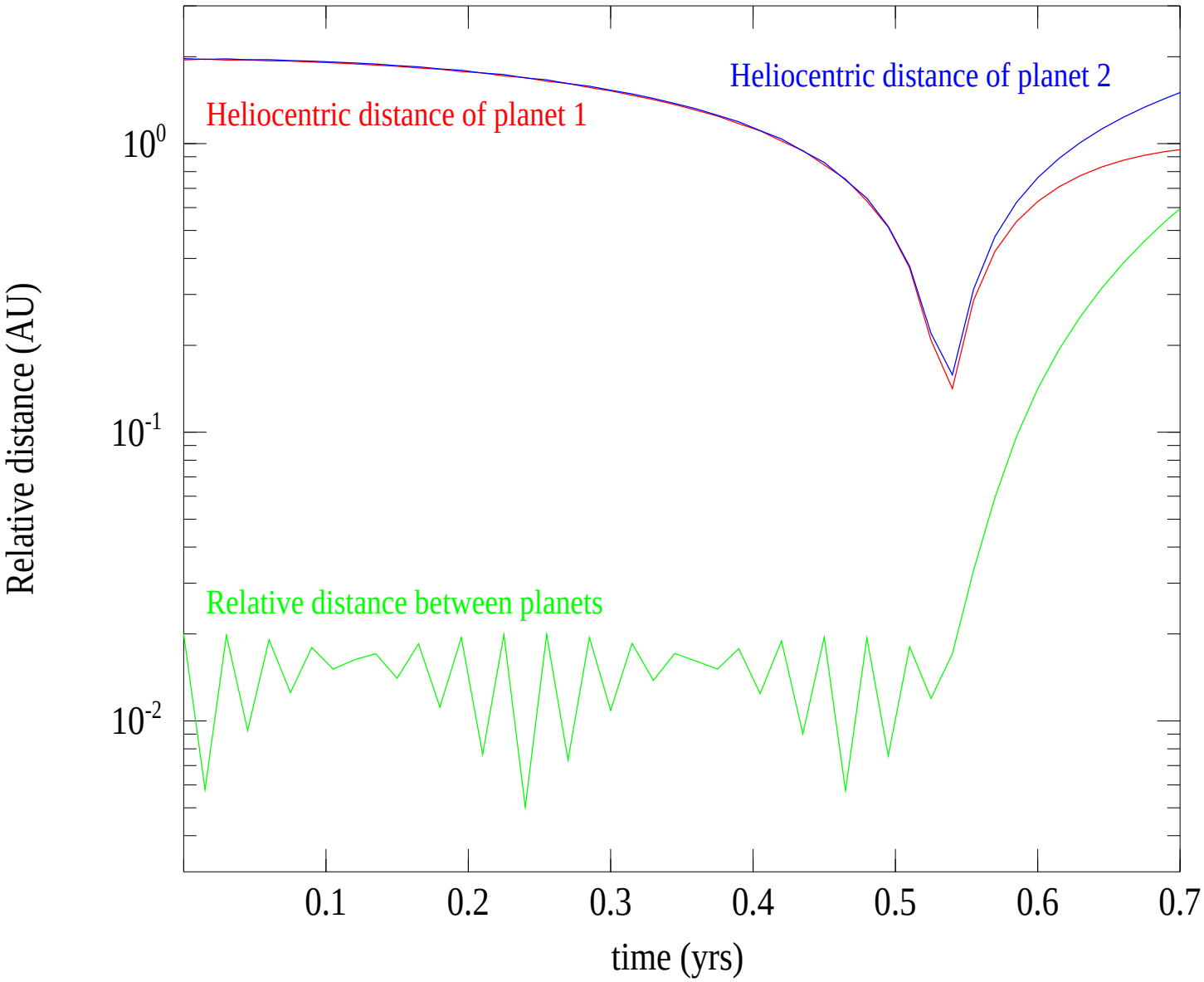
Heliocentric distance of planet 2
Heliocentric distance of planet 1
Relative distance between planets
Relative distance (AU)
10^0
10^{-1}
10^{-2}
0.1
0.2
0.3
0.4
0.5
0.6
0.7
time (yrs)

Figure6 —

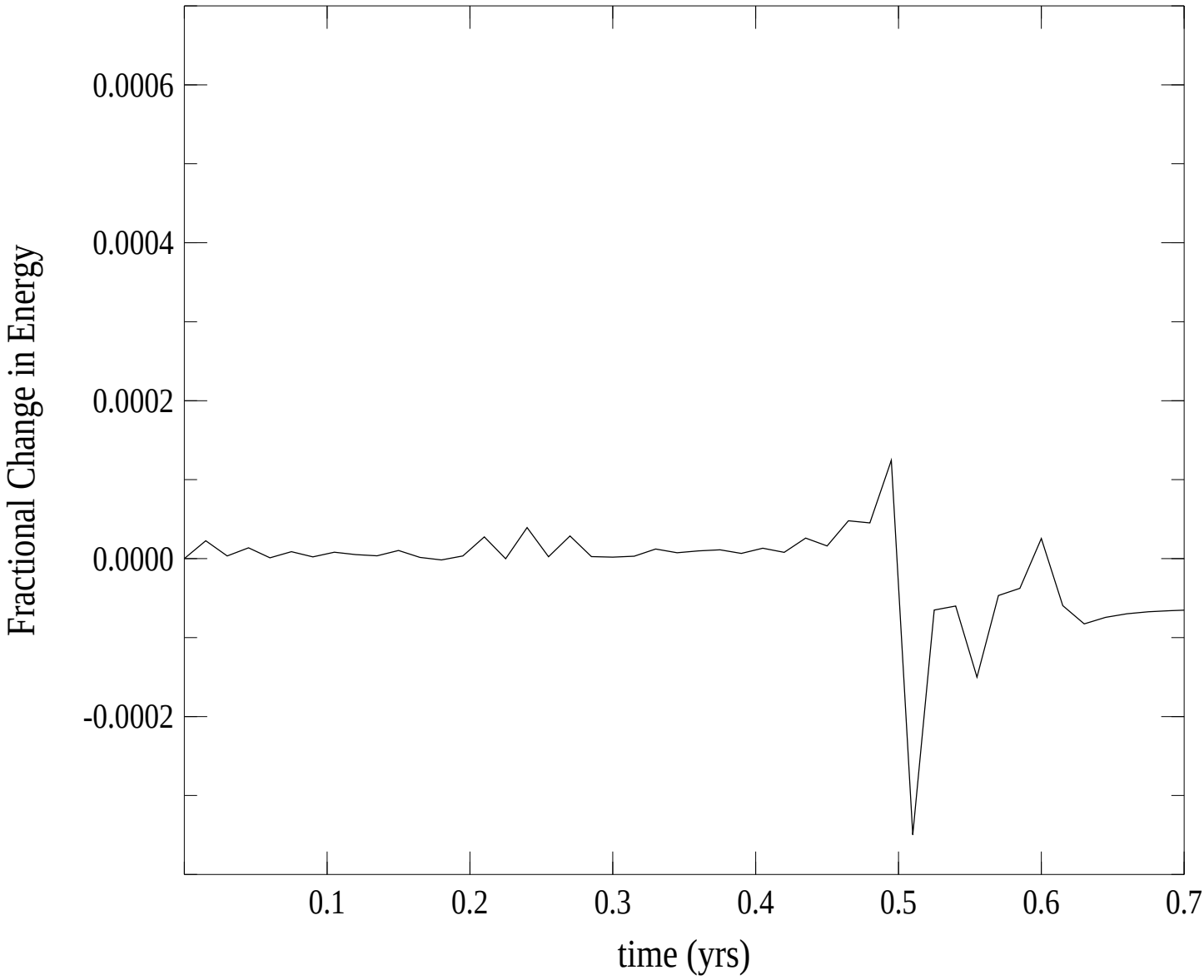
0.0006
0.0004
0.0002
0.0000
-0.0002
Fractional Change in Energy
0.1
0.2
0.3
0.4
0.5
0.6
0.7
time (yrs)

Figure7 —

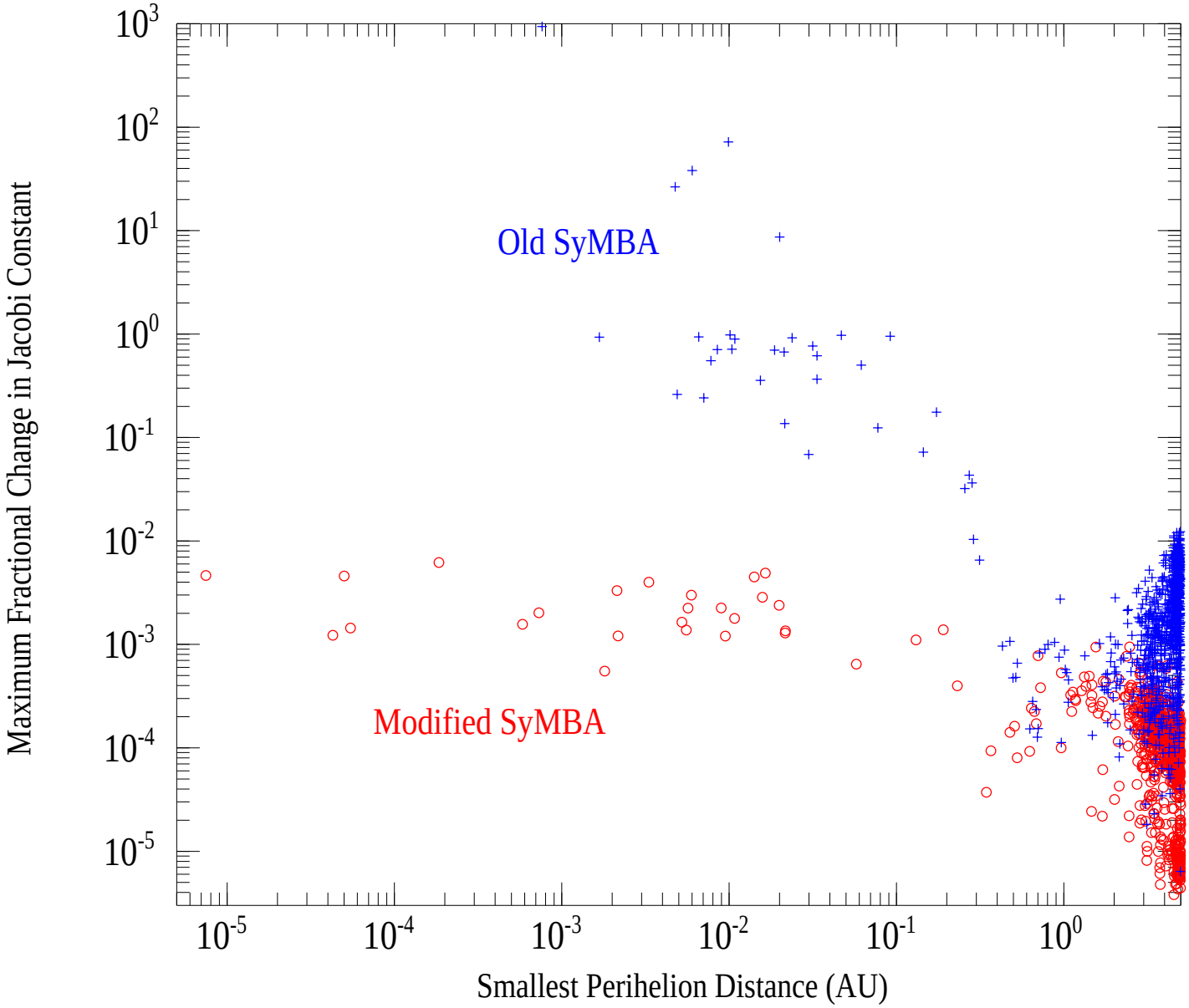
Maximum Fractional Change in Jacobi Constant
10^{3}
10^{2}
10^{1}
10^{0}
10^{-1}
10^{-2}
10^{-3}
10^{-4}
10^{-5}
Old SyMBA
Modified SyMBA
10^{-5}
10^{-4}
10^{-3}
10^{-2}
10^{-1}
10^{0}
Smallest Perihelion Distance (AU)